Multi-Phase Fracture-Matrix Interactions Under Stress Changes

Technical Progress Report
Semi-Annual

Reporting Period
March 21, 2001 – September 20, 2002

Principal Authors:

A.S. Grader, D. Elsworth, P.M. Halleck, F. Alvarado, H. Yasuhara,
A. Alajmi, Z. Karpyn

Report Issue Date: October 28, 2002

DOE Award Number: DE-FC26-01BC15355

Submitting Organization:

A.S. Grader
203 Hosler Building
The Energy Institute
The Pennsylvania State University
University Park, PA 16802

DISCLAIMER

ABSTRACT

The main objectives of this project are to quantify the changes in fracture porosity and multi-phase transport properties as a function of confining stress. These changes will be integrated into conceptual and numerical models that will improve our ability to predict and optimize fluid transport in fractured system. This report details our progress on **a**. *developing the direct experimental measurements of fracture aperture and topology using high-resolution x-ray micro-tomography,* **b**. *modeling of fracture permeability in the presence of asperities and confining stress*, and **c**. *simulation of two-phase fluid flow in a fracture and a layered matrix*.

The three-dimensional surface that describes the large-scale structure of the fracture in the porous medium can be determined using x-ray micro-tomography with significant accuracy. The distribution of fracture aperture is a difficult issue that we are studying and developing methods of quantification. The difficulties are both numerical and conceptual. Numerically, the three-dimensional data sets include millions, and sometimes, billions of points, and pose a computational challenge. The conceptual difficulties derive from the rough nature of the fracture surfaces, and the heterogeneous nature of the rock matrix. However, the high-resolution obtained by the imaging system provides us a much needed measuring environment on rock samples that are subjected to simultaneous fluid flow and confining stress. Pilot multi-phase experiments have been performed, proving the ability to detect two phases in certain large fractures.

The absolute permeability of a fracture depends on the behavior of the asperities that keep it open. A model is being developed that predicts the permeability and average aperture of a fracture as a function of time under steady flow of water including the pressure solution at the asperity contact points.

Several two-phase flow experiments in the presence of a fracture tip were performed in the past. At the present time, we are developing an inverse process using a simulation model to understand the fluid flow patterns in the presence of a fracture, and the interactions between fluid flow in the fracture and the adjacent matrix. Preliminary results demonstrate that the flow patterns are significantly impacted by the presence of the fracture. Bypassing is quantified and we expect to be able to extract from the modeling the distribution of properties in the fracture and the adjacent matrix.

TABLE OF CONTENTS

LIST OF FIGURES

INTRODUCTION

Natural and artificially-induced fractures in a reservoir have a great impact on fluid flow patterns and on the ability to recover hydrocarbons. In tight formations, the naturally fractured system provides access to the hydrocarbon fluids stored in the matrix. Fractures can have a negative effect on recovery processes when they form bypassing paths, especially in production-injection systems. For example, injected fluid may preferentially flow through the fractures leaving behind inaccessible and non-contacted hydrocarbons. Fractures can enhance the efficiency of displacement operations when the main direction of flow is perpendicular to the direction of the fractures. Fractures may also be non-conductive and form barriers to fluid flow. The mass transport between the fractures and the surrounding matrix has an important role in being able to predict and optimize the recovery processes from fractured reservoirs. As production occurs and pore pressures decline, the net confining stress on the rock increases. This project focuses on the effects that changes in confining stress have on the transport properties of the fracture-matrix system. The confining stress has an impact on the fracture aperture and therefore on multiphase fluid transport properties (*Barton et al.*, 1985, *Gentier et al.*, 1997). We propose to quantify the changes in fracture porosity and saturation distribution under steady and non-steady flow in both the fracture and the adjoining matrix. The quantitative changes will be obtained by low and high resolution X-ray computerized tomography (CT) imaging (*Vinegar and Wellington*, 1987), and then these changes will be used in an inverse simulation process to quantify changes in permeabilities and to suggest up-scaling procedures.

We propose a fracture-matrix interaction program with the following objectives:

• Quantify the effects of confining stress on fracture topology and aperture and porosity.

• Quantify the changes in two-phase fracture permeabilities as a function of stress.

• Determine the effect of stress on oil-water transport between the fracture and the matrix.

• Determine the effects of stress on recovery processes in the presence of fractures.

• Use inverse simulation of four-dimensional saturation data for up-scaling.

We approach multi-phase flow in stressed fractured rocks experimentally and computationally. We will use multi-phase injection into confined rock samples that contain natural fractures or artificially induced ones. We will quantify the saturation distribution temporally and spatially (four-dimensional) using our new imaging facility and The Center for Quantitative Imaging. We will also monitor the pressure behavior of the sample and confining fluids. The resulting four-dimensional distribution of saturations and pressure histories will form the basis for multi-phase fluid flow simulation with the ultimate goal of quantifying the changes in the fluid flow characteristics of the rock as a function of the net confining stress. This combined experimental/computational approach will lead to advances in our understanding of the effects in-situ stress on recovery processes.

EXECUTIVE SUMMARY

The main objectives of this project are to quantify the changes in fracture porosity and multi-phase transport properties as a function of confining stress. These changes will be integrated into conceptual and numerical models that will improve our ability to predict and optimize fluid transport in fractured system. The project has five tasks:
1. Quantify the effects of confining stress on fracture topology and aperture and porosity.
2. Quantify the changes in two-phase fracture permeabilities as a function of stress.
3. Determine effects of stress on oil-water transport between the fracture and the matrix.
4. Determine the effects of stress on recovery processes in the presence of fractures.
5. Use inverse simulation of four-dimensional saturation data for up-scaling.
This report focuses mainly on tasks 1, 2 and 5.

Fracture Topology, Aperture, and Fluids: Three new experiments were performed during this reporting period. In the first preliminary experiment, a fractured sandstone sample was tested in a tri-axial cell. The fracture aperture was between 50 and 200 microns. Initial results indicate that it should be possible to map the distribution of the two phases in the fracture. However, an increased CT contrast between the fluids is needed. In the second experiment, a fractured limestone sample was used with tagged oil and non-tagged water. The high-resolution images presented a clear distinction between the oil and the water. Even the oil/water interface within the fracture was clearly observed. These experiments pave the road to a new set of experiments to be performed in the pressure vessel.

Modeling of Fracture Closure: There is much literature treating a fracture as a gap between two parallel plates. We have been of the opinion that most fractures are far from such a description, and have rough walls with asperities that maintain keep the fracture from closing. Also, the fracture topology is not a single plane, and has significant variations. We are developing a model that can describe the effective fracture aperture, and thus fracture permeability, as a function of time under various histories of confining pressure, temperature, and the rate of water flow. We observe that increasing the temperature accelerates the pressure solution of the asperities and allows the fracture to close and reduce the absolute permeability. The solution and deposition model is near completion.

Modeling of Fracture-Matrix Fluid Flow Interactions: Some previously performed two-phase flow experiments are being analyzed. In one of these experiments, a layered sample was fractured at the inlet end, with an axial fracture that extended only to the middle of the sample, creating a fracture tip. The oil loading process is being modeled. Two dimensional simulations are being integrated into a full three-dimensional model. Properties from the two-dimensional systems are used as the starting point for the three-dimensional simulations. Early results indicate that there is cross flow between the layers during the oil loading period.

EXPERIMENTAL SYSTEM

The experimental system used in this project includes a multi-phase fluid flow system, a core holder assembly that can provide controlled confining pressure, and an x-ray computed tomography system. A schematic of the system is shown in Figure 1 and photographs of the medical and the industrial scanners are shown in our first quarterly report. Most of the details of the fluid flow system can be found in *Alajmi and Grader* (2000). Two new core holders were acquired. These are tri-axial cells with high pressure ratings and elevated temperatures. The rock samples may have a diameter of up to 25 mm and a length of up to 300 mm. These core holders will be used to study the effects of confining stress and fracture aperture on two phase flow.

The Computed Tomography (CT) system consists of an ionized x-ray source, a detector, a translation system, and a computer system that controls motions and data acquisition. The x-ray source has a Tungsten target with a focal spot of 5 microns. It produces a cone beam that passes through the core and activates the detector. The image intensifier detector surface releases electrons that are then focused on a screen that is photographed by a high-resolution (1024x1024) camera with a frequency of 15 Hz. The sample is rotated 360 degrees in the x-ray beam while the detector is providing attenuation views to the data acquisition computer. After the sample is rotated a complete turn, the system reconstructs a slice, a cross-sectional image of the attenuation values that represents a combination of the density and the apparent atomic number of the sample and the imaged position. The imager operates in volume mode where several separate slices are collected in one rotation. In the example shown in the report, up to 41

slices were acquired in a single rotation. After each rotation, the sample is translated axially to a new scanning position, thus, allowing a continuous three-dimensional coverage of the sample.

The two experiments that are presented in this report demonstrate that it is possible to detect two phases in a fracture. The **first experiment** was performed with the fractured sample in a pressurized core holder with two-phase displacement. The **second experiment** was static with a wide aperture fracture.

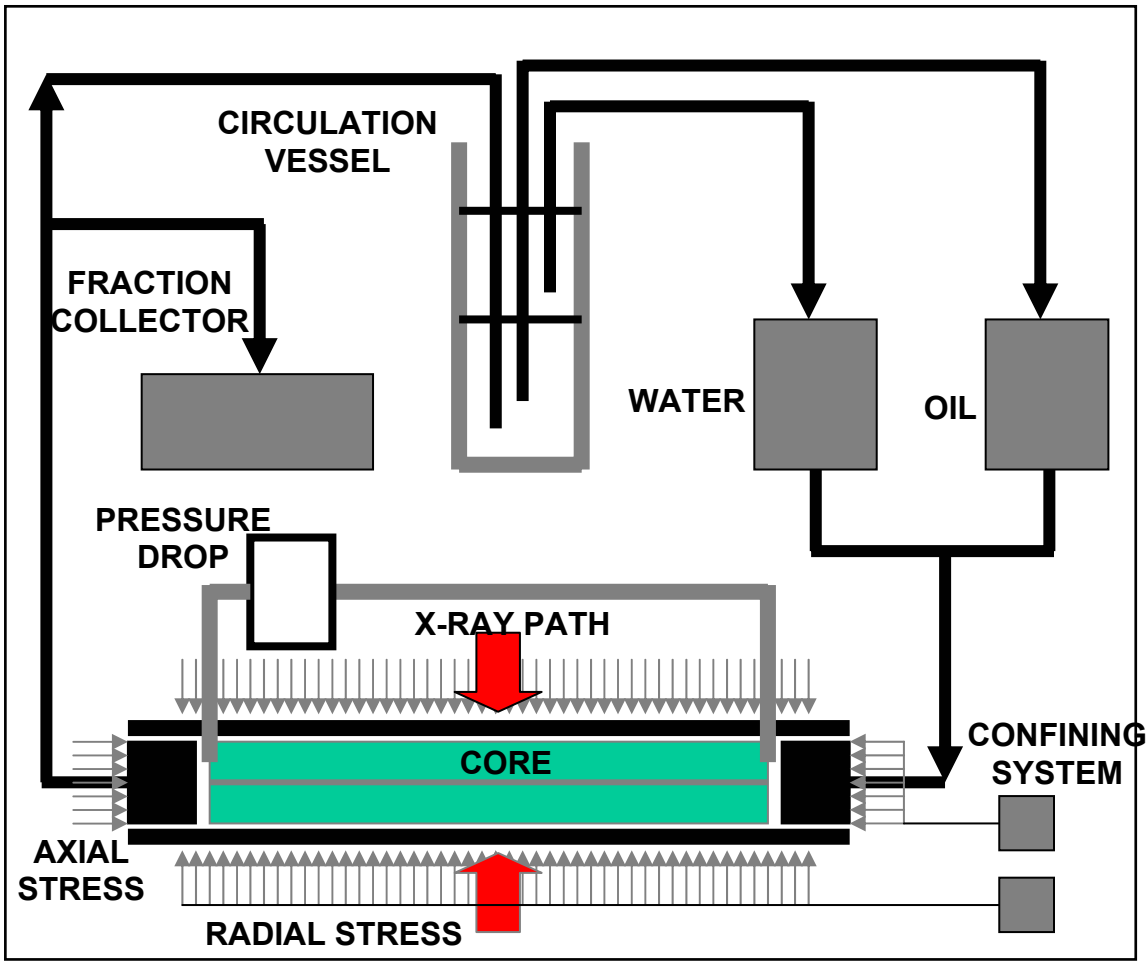

Figure 1: A schematic diagram of the fluid flow and rock sample apparatus.

RESULTS AND DISCUSSION

Fracture Topology and Aperture: Preliminary Experiment in the Tri-Axial Cell

The main goal of this experiment was to demonstrate the ability to detect two phases in the fracture using Computed Micro Tomography (CMT). The sandstone sample had a diameter of 25 mm and a length of 100 mm. It was fractured artificailly prallel to its long axis and its layers. The two parts of the sample were not opened yielding a fracture with a small aperture. The ends of the sample were trimmed to fit the end plugs of the core holder. The experiment was carried out in a vertical orientation with the fluids flowing in the upward direction. Fluids were injected only into the fracture. The following stages were performed:

1. Mount the sample and scan it under dry condirions.
2. Apply a vacuum to the sample and saturate with non-tagged water.
3. The sample was scanned saturated with water.
4. Inject tagged oil to displace the water out oif the fracture.
5. The sample was scanned at residual water saturation in the fracture.
6. Water and oil were injected at steady conditions.
7. The sample was scanned during steady state flow.
8. Injection was stopped, allowing counter-current flow to occur.
9. Several confinig pressures were applied.

This report focuses on the first seven stages of the experiment. Figure 2 shows a single image through the dry sample. The gray-scale image highlights the width of the fracture and several asperities. The colored image shows the fracture in shades of blue, denoting the large apertures in dark blue.

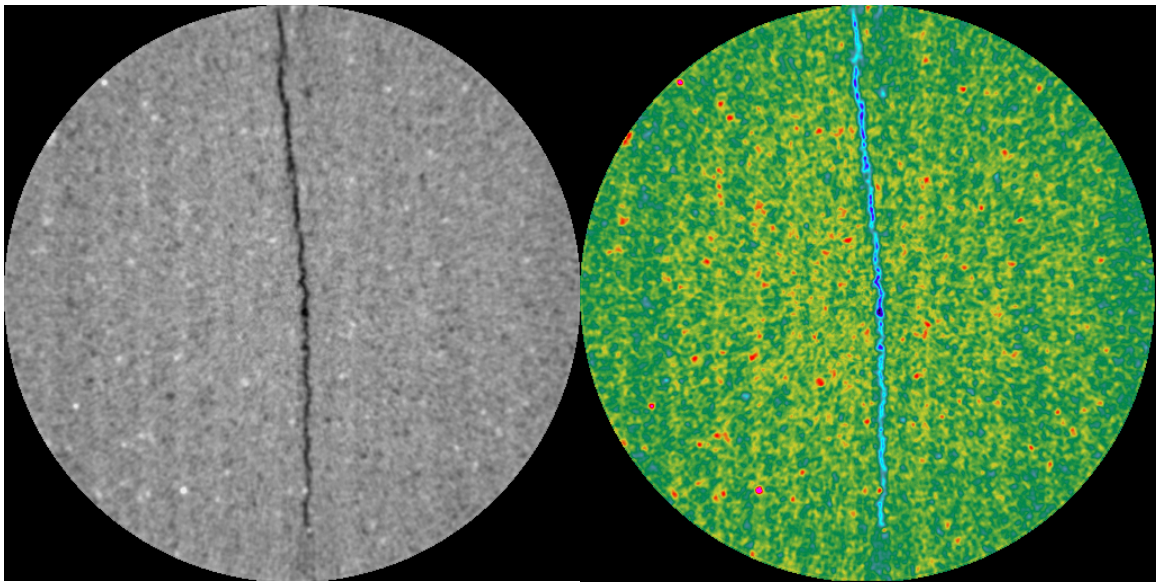

Figure 2: A typical slice through the sample. The diameter is about 20 mm. The slice shows the fracture parallel to bedding.

A total of 492 images were acquired with a resolution of about 30 microns in all dimension. Figure 3 shows an axial section through the sample showing the fracture. At one end of the sample a cross-fracture developed during the fracturing procedure. It appears as the dark horizontal region at the lower part of the figure.

A detailed view of the fracture in a single image is shown in Figure 4. The image on the left is the complete image and the highlighted box is expanded on the right. The detailed image clearly shows one of the asperities that is keeping the fracture open. A repeat set of images was acquired after the sample was fully saturated with water. Figure 5 shows the same an image and a detailed region as in Figure 3, but fully saturated. It is difficult to detect the presence of the water without image subtraction. Figure 6 shows a subtracted image with the net presence of water in the fracture. The subtracted image was windowed so that the water in the fracture is clear. Figure 7 shows the net water in an axial section of the sample. The distributed white speckles represent water in individual pores in the sandstone.

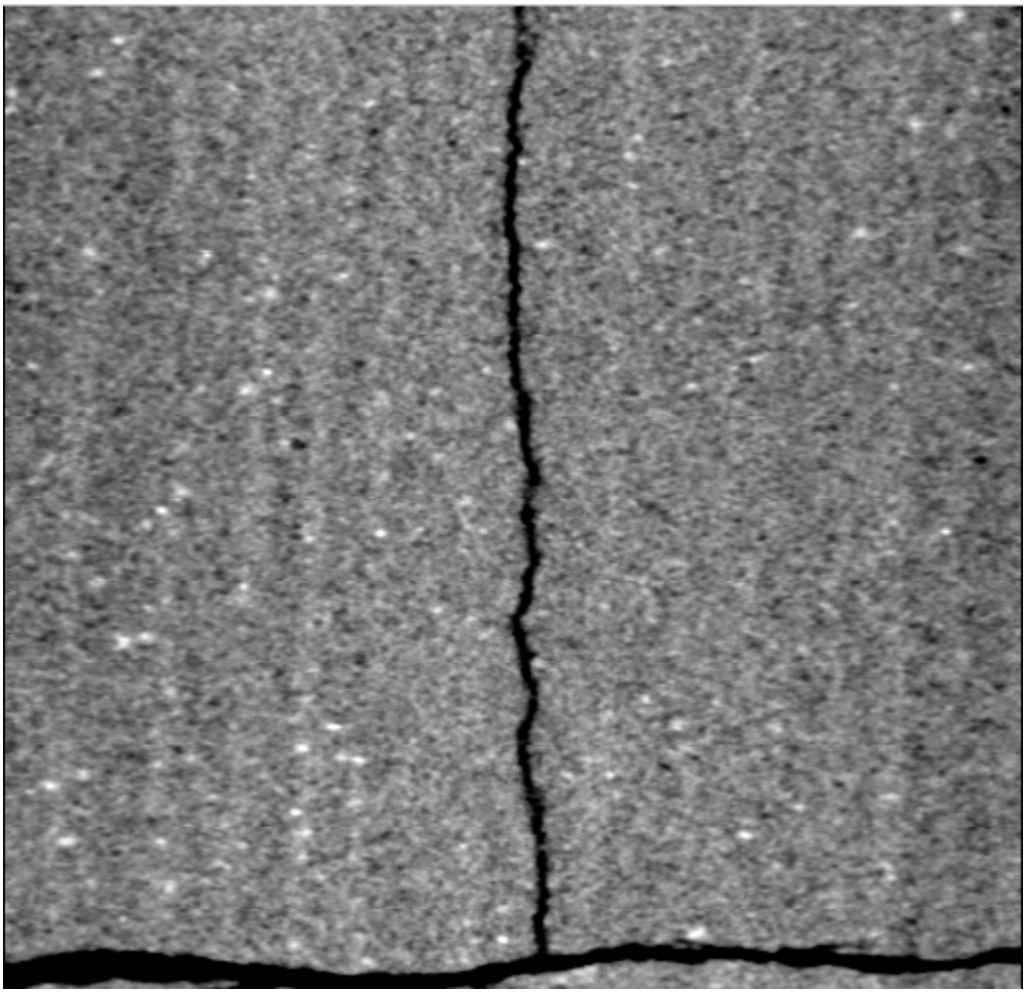

Figure 3: Axial section along the sample. The dark shade represents the fracture.

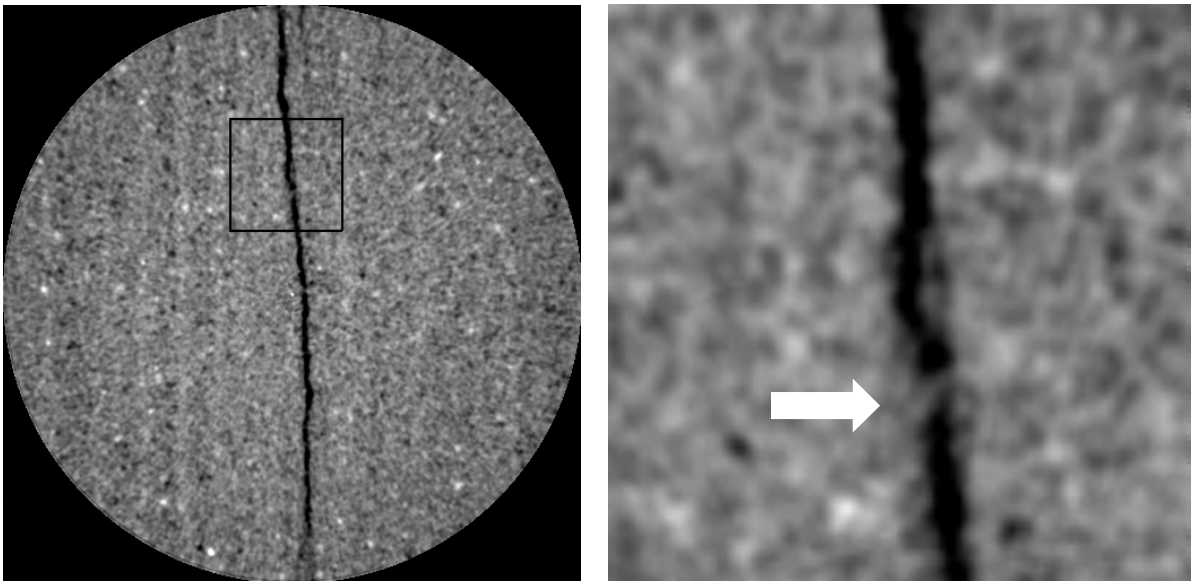

Figure 4: An expanded view of the dry fracture in a single image, showing an asperity.

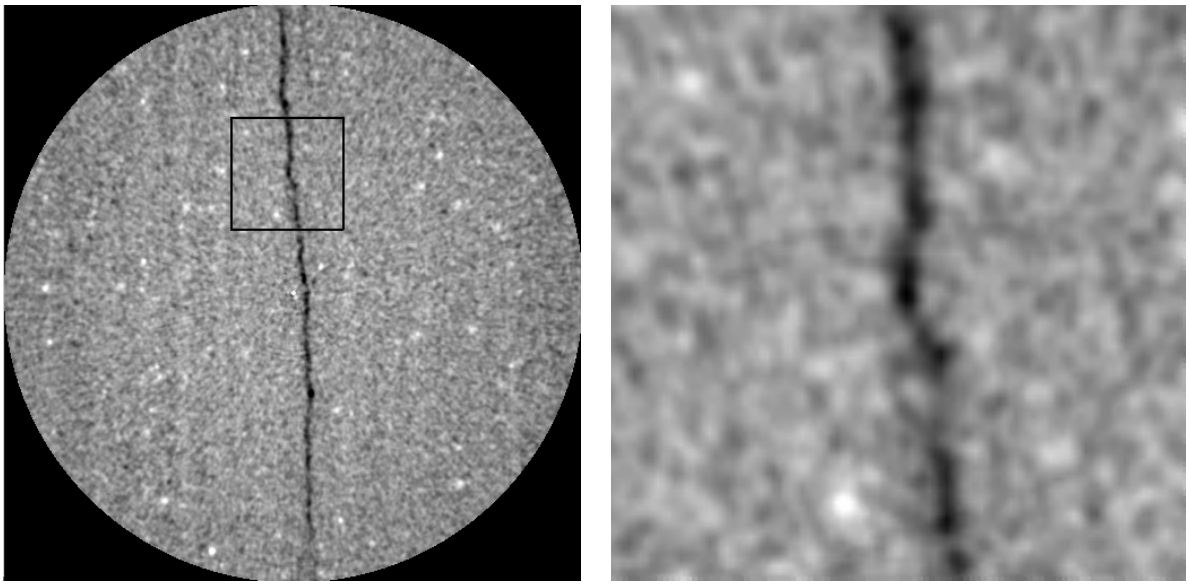

Figure 5: An expanded view of the fracture in a single image, showing an asperity. The sample is fully saturated with water. The fracture width is between 100 and 200 microns.

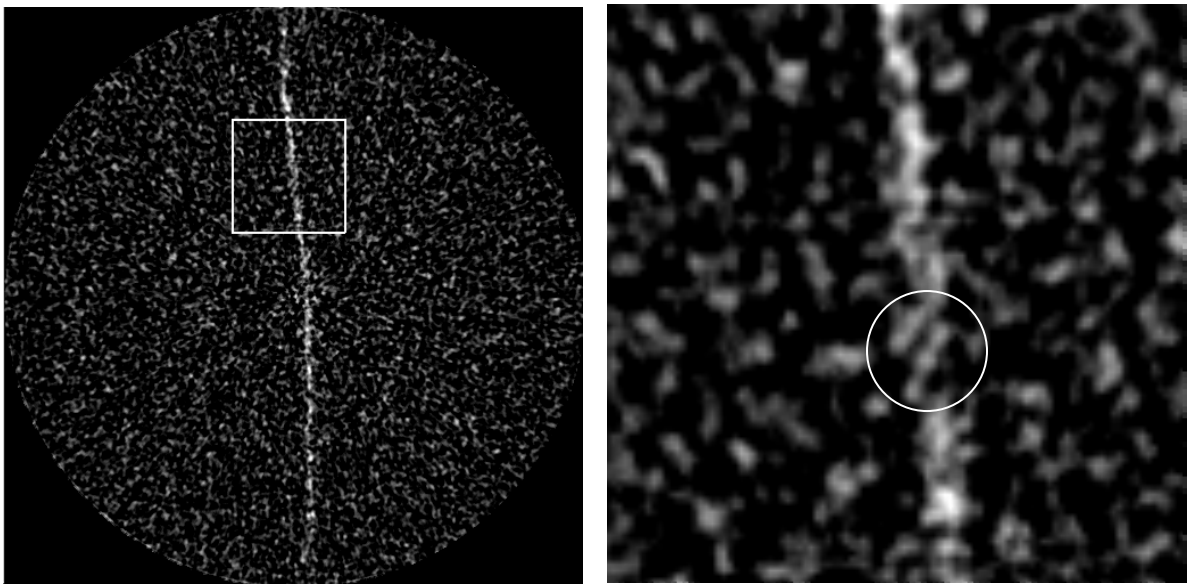

Figure 6: An Image of the net water in the sample, windowed to amplify the presence of water in the fracture (white streak in the middle of the sample). The sample is fully saturated with water. The circle identifies the asperity.

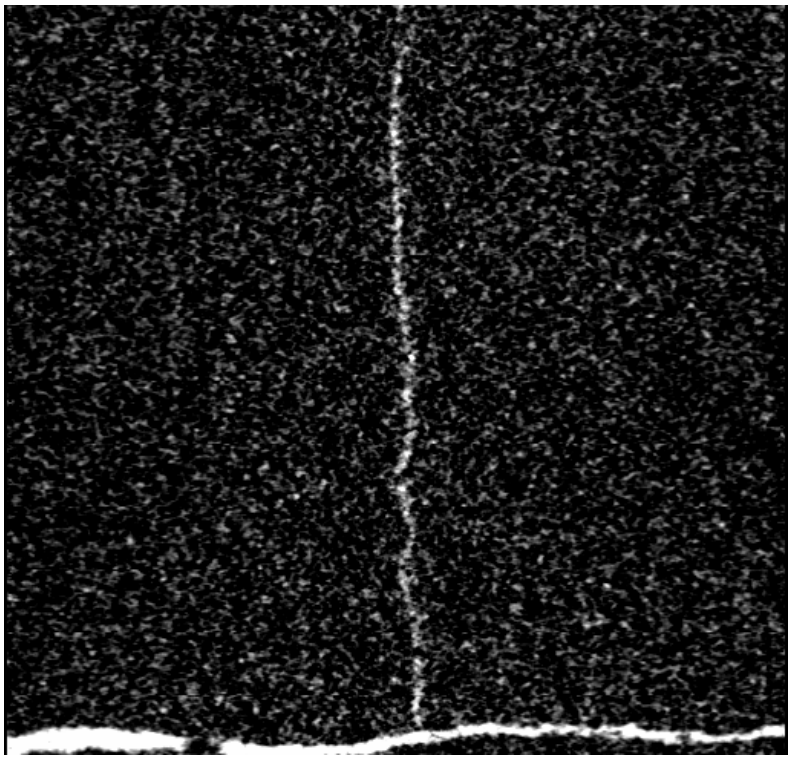

Figure 7: An axial view of the net water in the sample, windowed to amplify the presence of water in the fracture (white streak in the middle of the sample). The sample is fully saturated with water.

After the sample was fully saturated with water, oil was injected to displace most of the water out of the fracture. The silicone oil was mixed with iodododecane, to reduce its viscosity and to increase its x-ray signature. The fully water saturated images were subtracted from the oil saturated ones. Figure 8, left, shows a single subtracted image where the presence of oil is denoted by the black regions. An axial section through the core is shown on the right side of Figure 8. The presence of oil in the fracture is visible. The horizontal line in the image passes through one of the large fracture apertures, where a significant amount of oil is present. Figure 9 shows a profile along this horizontal line. The black line denotes dry conditions. The read line denotes a fully water saturated sample. The blue line denotes the oil saturated sample after displacing the water. The increase in CT values in the fracture between the wet and dry conditions are significant and are grater than the increase in the matrix region. The further

increase in CT values in the fracture between the dry and water-saturated and oil-saturated conditions is evidence that the oil can be detected in the fracture. There is little increase in oil saturation in the matrix, as expected since the fracture spans the entire sample. Further processing should allow us to map the distribution of the oil and the water in the sample, and later on, relate this distribution to saturation and to relative permeabilities.

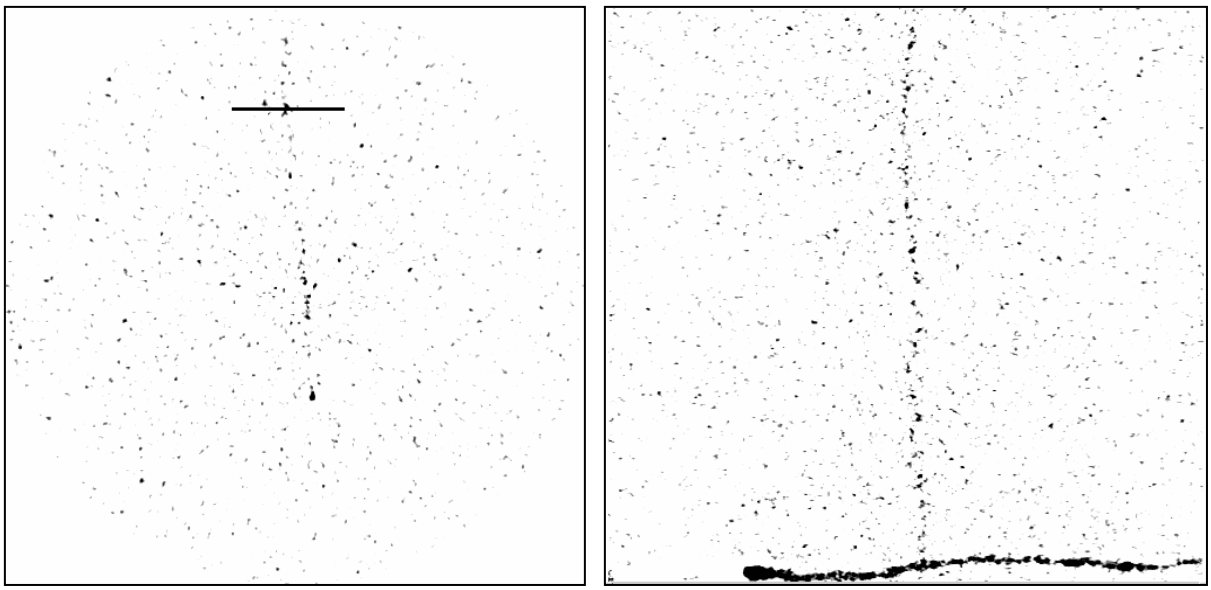

Figure 8: An image (left) and an axial section (right) showing the net presence of oil in the sample. The presence of oil in the fracture is clearly visible.

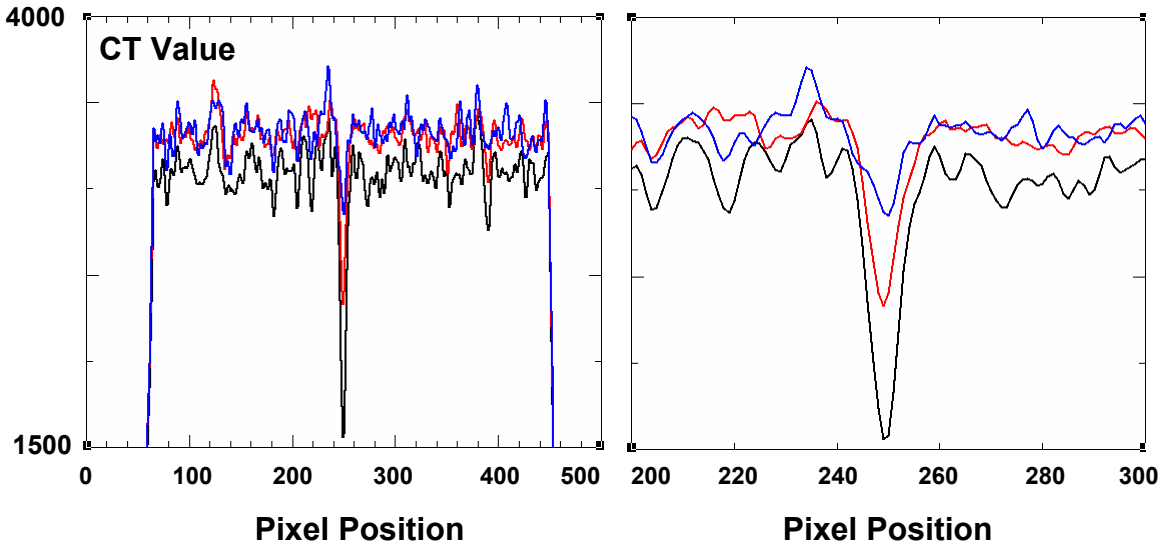

Figure 9: Profiles through the fracture that contains oil. The figure on the right is an expanded range of the central part of the figure on the left.

Fracture Topology and Aperture: Two Stationary Phases in a Fracture.

This experiment was performed in order to determine the level of fluid contrast needed to separate the fluids in a relatively large fracture. A limestone sample with a diameter of 50 mm was fractured and trimmed. It was placed in a heat-shrink Teflon tube and placed on a Teflon end cap to provide a fluid seal, shown in Figure 10. The brass strip attached to one side of the fracture serves to reduce the intensity of the x-ray beam when it is aligned with the fracture. The Teflon end cap was placed in the scanner in a vertical orientation as shown in Figure 11. Figure 12 shows a photograph of the limestone sample in book format. This photograph demonstrates that the fracture does not have smooth flat walls. Figure 13 shows a detailed region of the sample with a small shell. The dry sample was scanned at a resolution of about 50 microns in all dimensions. A typical image is shown in Figure 14, left, and a detailed portion of the fracture is shown to the right. The high-resolution shows the edges of the fracture as well as the uneven nature of the surface. The sample was saturated with non-tagged water, and then a portion of the fracture was filled with tagged oil. Figure 15 shows that the two fluids are clearly distinguished in the scan. Even the capillary interface between the water and the oil is properly detected as shown by the enlarged detailed image on the right. In this figure, water is denoted by the green color and oil by the red color. The fracture was propped with silica sand grains of about 0.8-1.0 mm. One of these grains is seen in the detailed photograph in Figure 13. An axial section through the fracture is shown in Figure 16. The oil/water interface is shown on the left side of the section. Since the fracture is not parallel, the axial section intersects the matrix as well as the fracture, yielding the scattered red objects that are not oil.

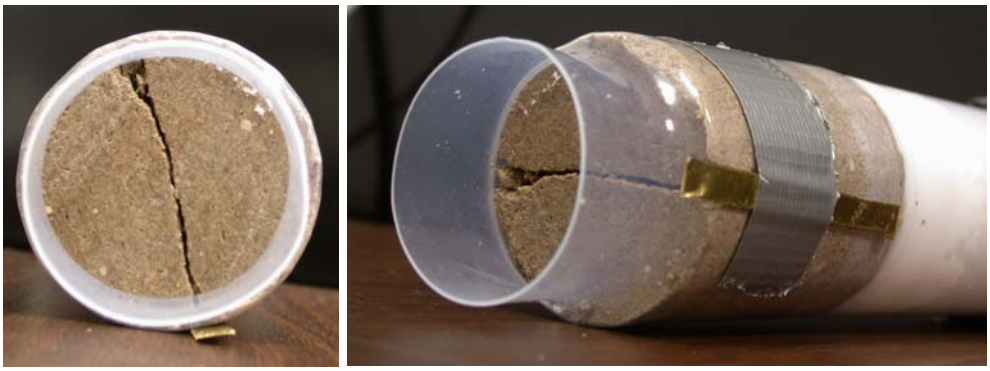

Figure 10: Photographs of the fractured limestone sample.

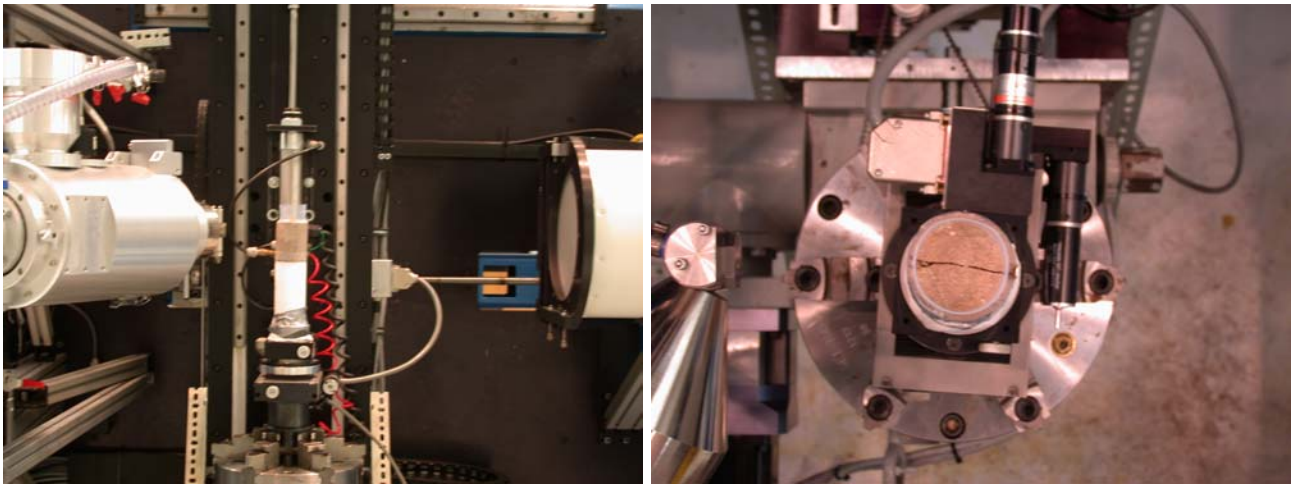

Figure 11: Photographs of the fractured limestone sample mounted in the OMNI-X high-resolution scanner. Left: horizontal view. Right: Vertical view.

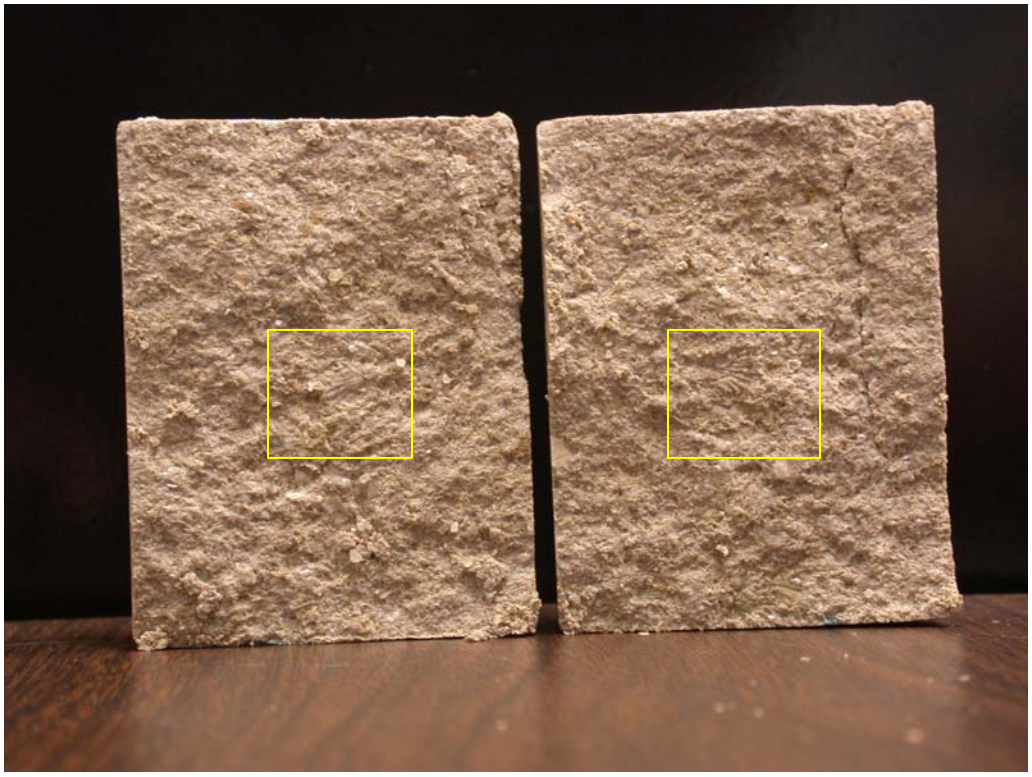

Figure 12: Photographs of the fractured limestone sample in book format.

Figure 13: Photographs of a detail the fractured limestone sample in book format showing a shell.

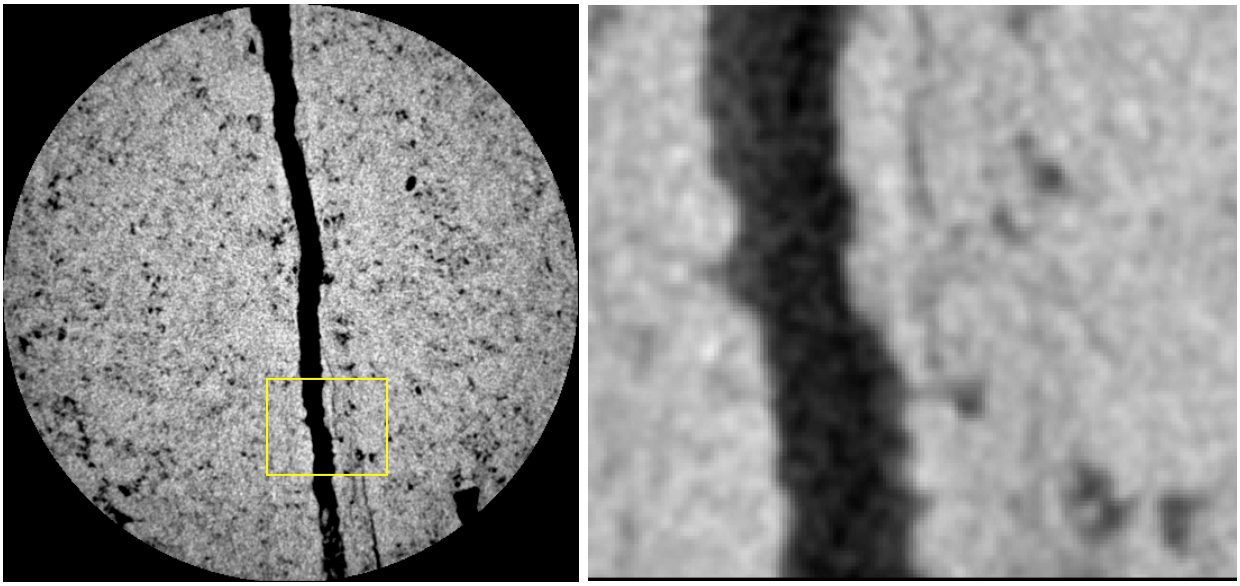

Figure 14: A CT high-resolution image through the limestone sample. Left: entire image. Right: a magnified detail of the fracture.

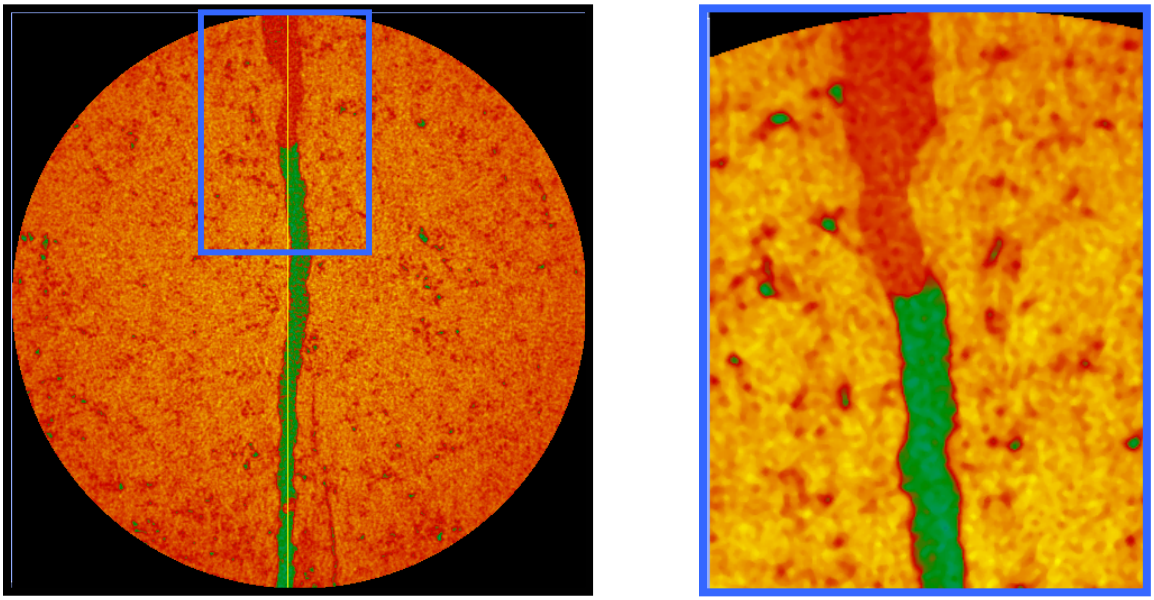

Figure 15: A CT high-resolution image through the limestone sample. Left: entire image. Right: a magnified detail of the fracture. Green: water. Red: oil.

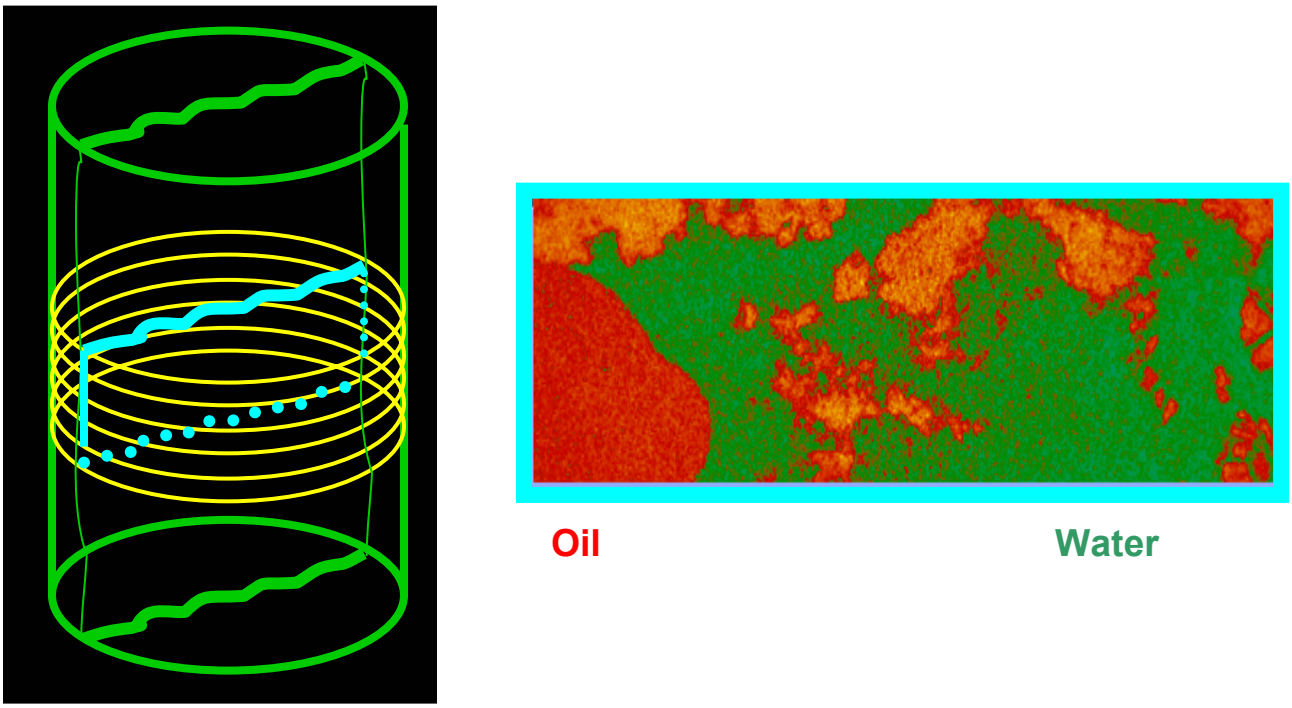

Figure 16: An axial section of the limestone sample through the fracture showing the oil/water interface. Water: green. Oil: red.

The OMNI-X scanner has the capacity to produce images with various resolutions. The quality of the images depends on parameters such as the combined kV and mA energy levels, filtering, the number of views (acquisition time), the location of the sample with respect to the source and the detector. Figure 17 shows an example of three images with different qualities of the same location in the sample. The resolution is selected based on the individual experiment. The oil/water interface is well defined in the 4800 views image.

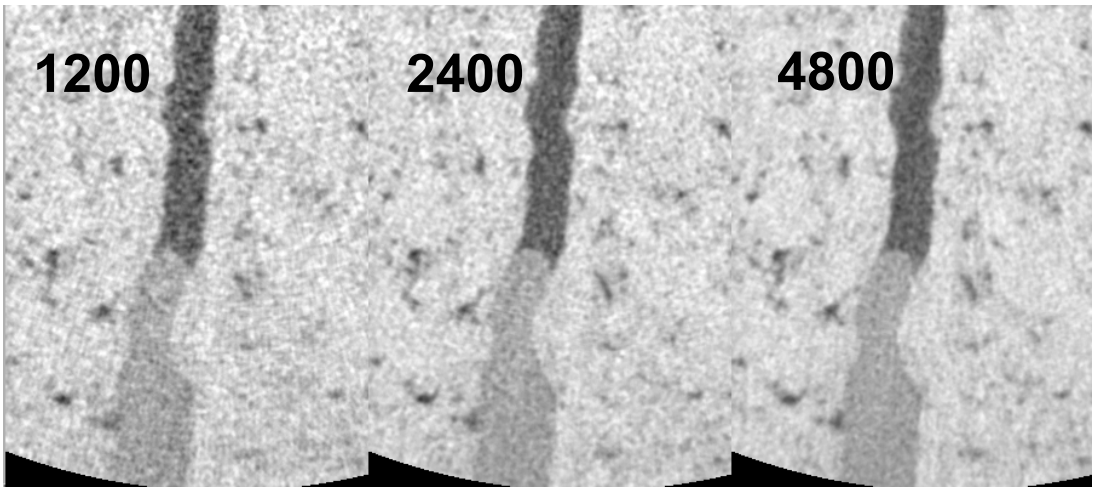

Figure 17: Three identical images with differing resolutions. Left: 1200 views. Middle: 2400 views. Right: 4800 views.

This experiment demonstrates that we should be able to determine the distribution of the two fluids in the fracture. In the next experiment, the same fluids will be used to inside the pressure vessel to determine the effect of the aluminum core holder wall on the ability to separate the two fluids.

A second experiment testing the ability to detect two phases in a single fracture within a high pressure vessel was conducted using Berea sandstone. A 25 mm diameter sample was fractured using a modified Brazilian test, shown in Figure 18 in book format. The artificial fracture was oriented parallel to the natural bedding of the rock. The sample was placed inside an aluminum tri-axial pressure cell, shown schematically in Figure 19, and installed in the OMNI-X industrial scanner, Figure 20. Photographs of the limestone and the sandstone are shown in Figure 21, demonstrating the contrast between the textures of the fracture surfaces.

Figure 18: Fractured Berea sample in book format.

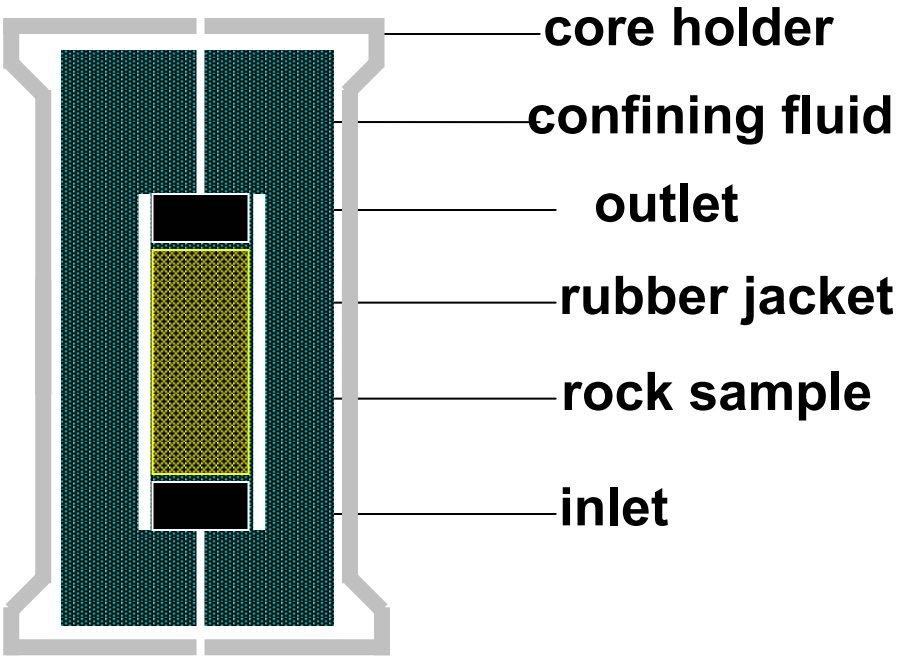

Figure 19: Schematic of the pressure vessel and its various components.

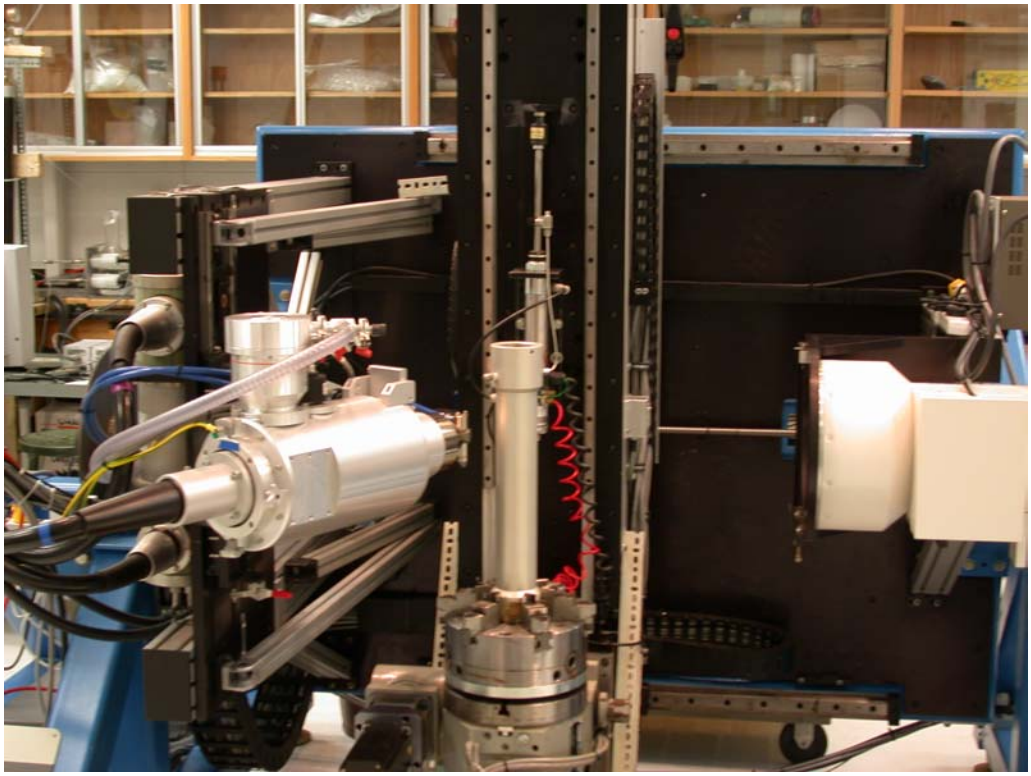

Figure 20: Photograph of the pressure vessel in the OMNI-X scanner.

Figure 21: Photograph the Limestone and the Berea fracture faces.

The sample was scanned under dry conditions. Water was pumped into the sample and the entire matrix and fracture were saturated. During the filling of the sample with water, scans were acquired showing the air water interface. Then oil was introduced from the top and water was allowed to drain from the bottom, thus allowing oil to penetrate the fracture. Again, the sample was scanned. Scans of the various fluids in the fracture are shown in Figure 22 in two color scales. The top four images are in color and the bottom images are in black and white gray scale. Figure 23 shows a single image and a detail of the water-air interface. Capillary forces force the water to reside in the narrow portions of the fracture, wetting the face of the rock, as can be seen by the curvature of the water/air interface. There is a balance between gravitational and capillary forces that create a stable column of water adjacent to an air column. A water/oil interface is shown in Figure 24. Again, as the water is the wetting phase, it occupies the narrow portions of the fracture. A region of about 20 mm along the sample was scanned. Axial views through the sample at different fluid injection stages are shown in Figure 25. The water/air and water/oil interfaces in the bottom two views are clearly observed.

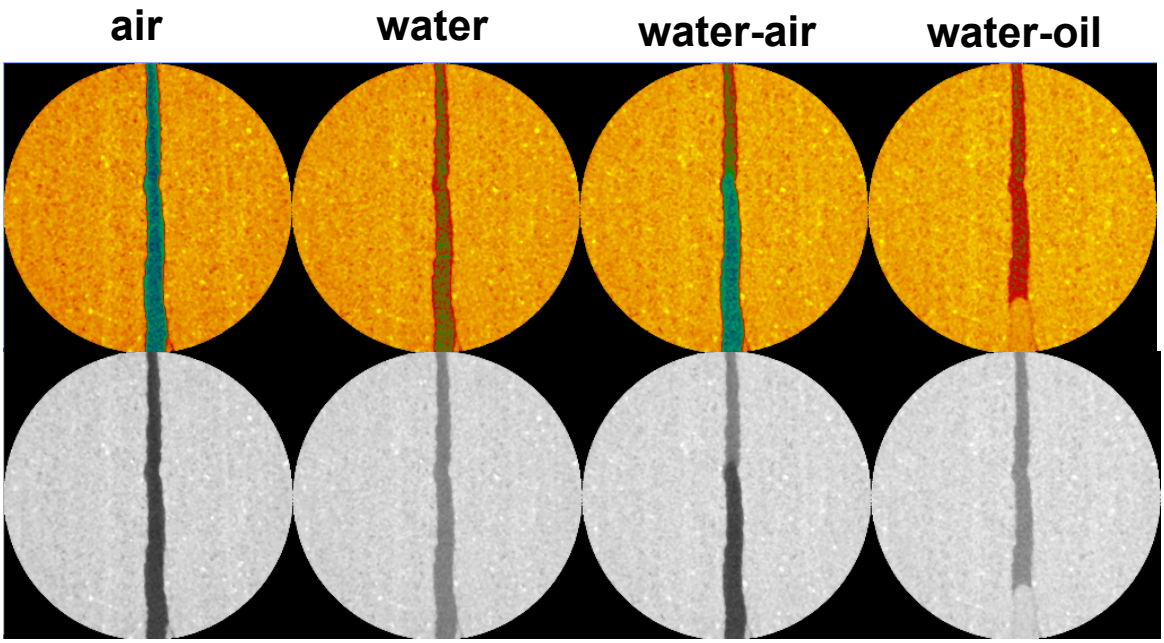

Figure 22: images showing air, water, water-air, and water-oil in the fracture.

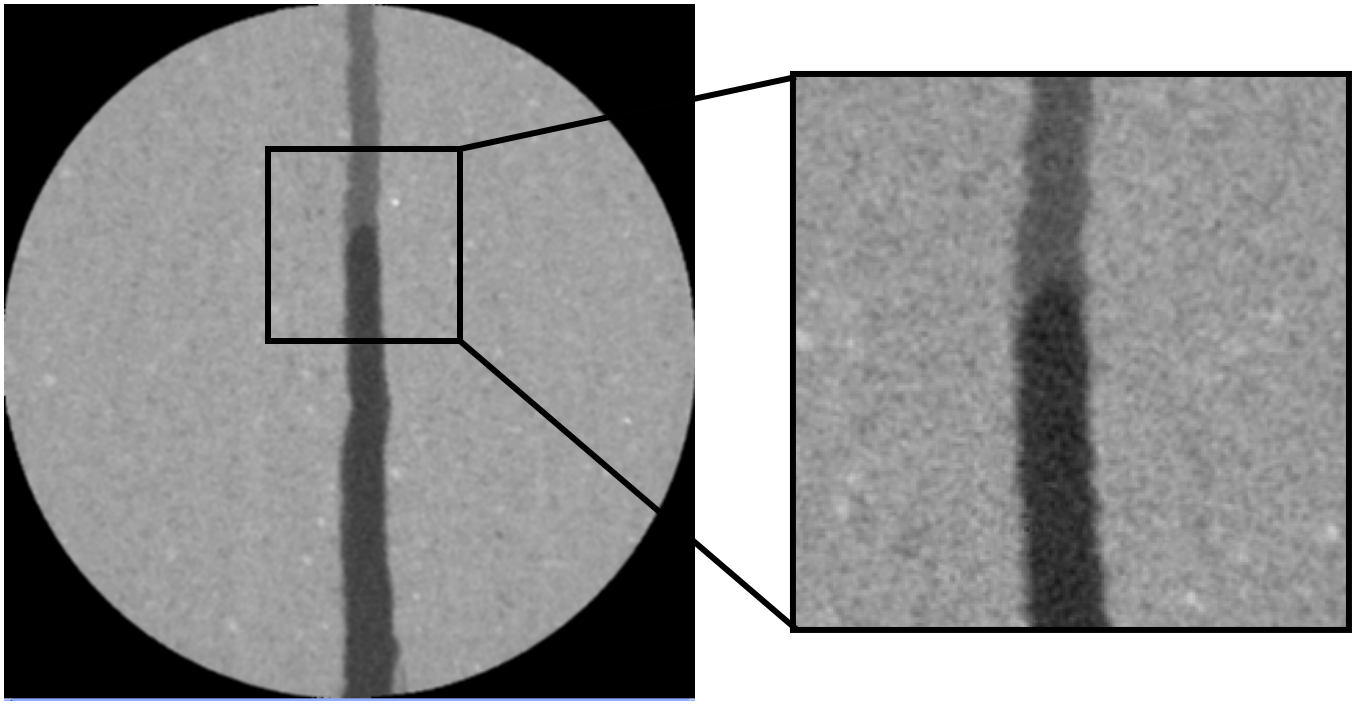

Figure 23: Image and detail showing a water-air interface.

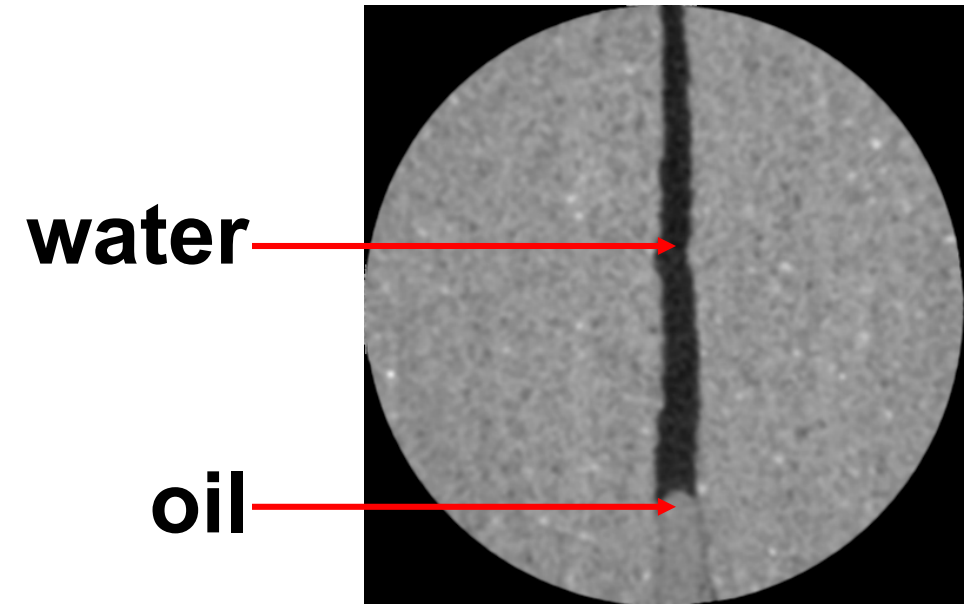

Figure 24: Image and detail showing a water-oil interface.

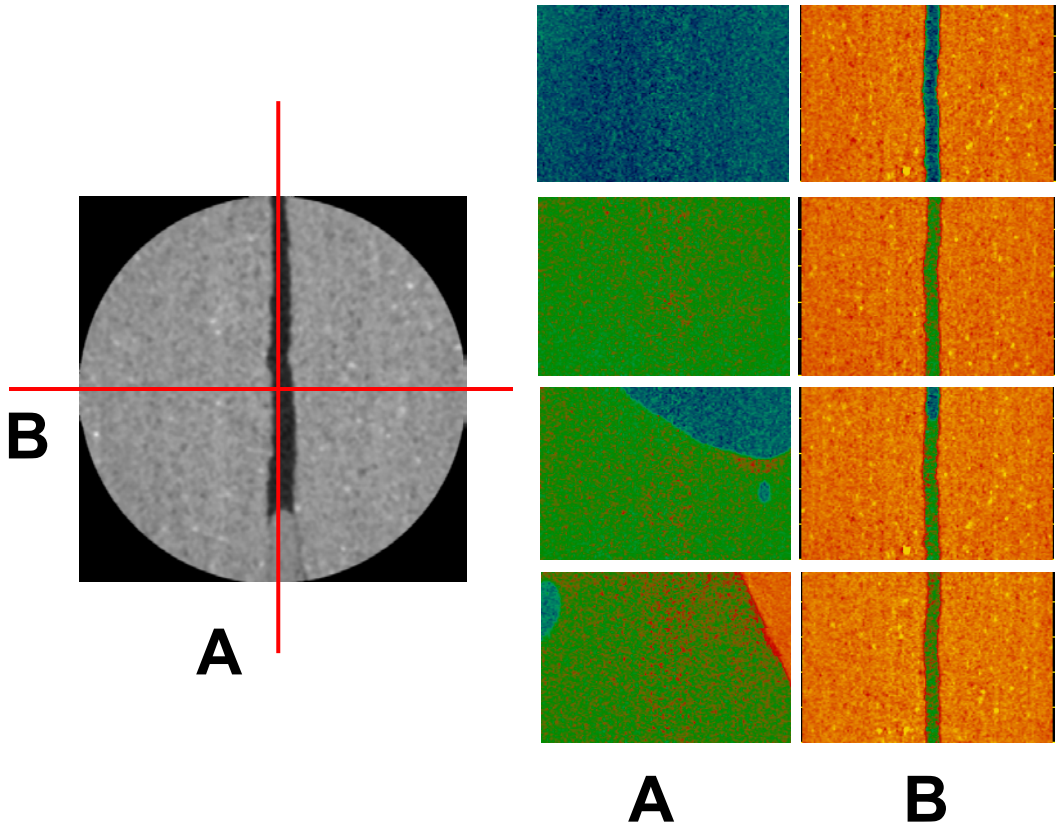

Figure 25: Axial views perpendicular to the fracture (B) and within the fracture (A).

Fracture Aperture Distribution:

A cylindrical Berea sample was cored parallel to the natural bedding with a diameter of 50 mm and a length of 200 mm. This sample was fractured perpendicular to bedding and then over-cored to a diameter of 25 mm, to reduce edge effects. The two halves of the sample were shifted by 1 mm along the axial axis, and then put together and scanned. The scanned region presented in this report had a length of 30 mm and a width of 16 mm. A total of 1394 scans were acquired at a voxel resolution of about 20 microns. A typical image of the sample is presented in Figure 26, with an expanded detail of the fracture on the right. The image shows the vertical layers and the expanded region shows large pores (black spots), high density elements (white spots) and the fracture. Through numerical processes that include erosion and dilation, a two-dimensional map of the distribution of fracture aperture was extracted from the entire data set, shown in Figure 27. The red areas are asperity regions where the two sides of the fracture are in contact. The white regions are regions of high fracture width of about 1200 microns. The yellow contour represents a fracture width of 600 microns. This type of analysis permits the computation of fracture volume, as well as to demonstrate the topology of the fracture. Dark regions would be filled with water, and light colored regions will form oil flow channels. We expect to perform fluid flow experiments in similar fractured samples. The pre-determination of the fractured region will simplify the partitioning of the two phases in the fracture during the post-acquisition analysis stage.

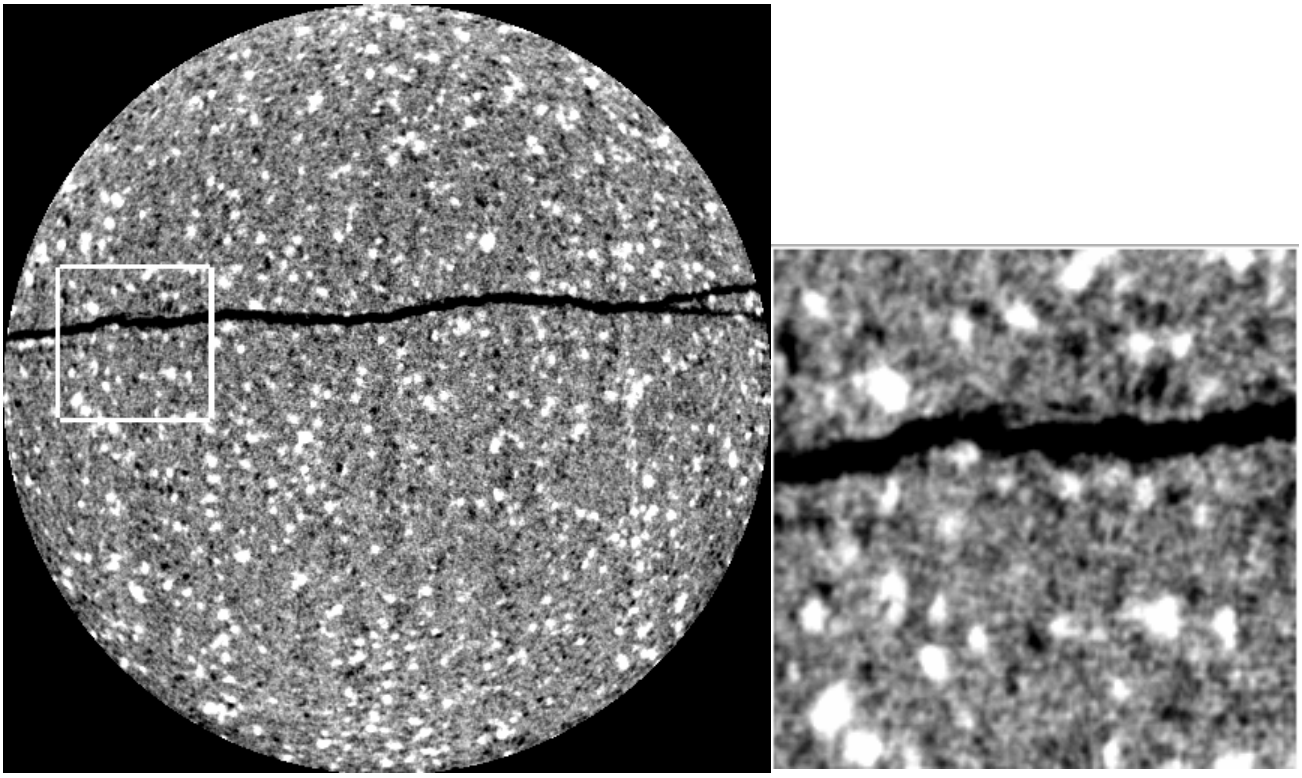

Figure 26: Fractured Berea sample and a detailed inset.

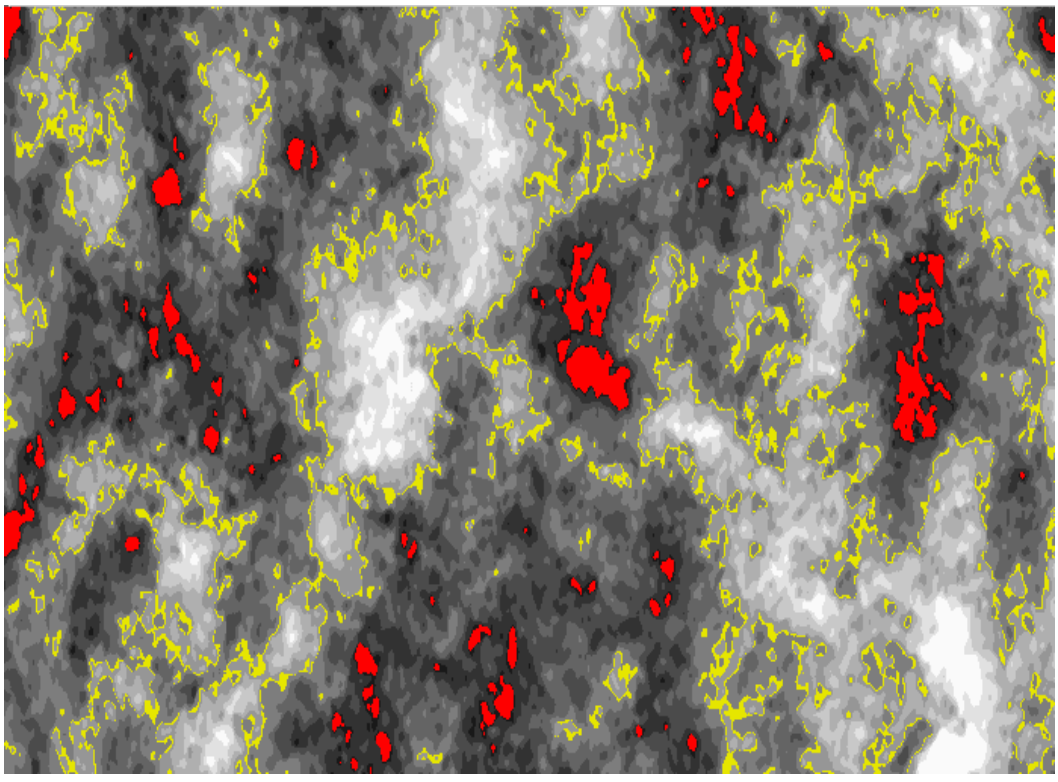

Figure 27: A two-dimensional map of fracture aperture. Area: 16mm x 30 mm.
Red: Contact regions. White: aperture of 1200 microns. Yellow: 600 microns contour.

New Core Holder Design:

The three experiments described in this report demonstrate the ability to detect fluids in a fracture with an aperture of 300 microns and above. A new low-pressure core holder was designed and built for studying the distribution of fluids in the fracture with fixed spacing and without modification of confining pressure. Once the technique of mapping the topology of the fracture and the fluid is established, similar enhancements of the high-pressure core holder will be made to study the effect of confining pressure and varying fracture apertures.

Photographs of the new core holder are shown in Figure 28. Confining pressure applies radial stress on the sample, and axial positioning is mechanical. The polycarbonate core holder sleeve can accommodate a 25 mm diameter sample up to a length of 150 mm (Figure 28A). Samples that are shorter than 150 mm require additional spacers. Each end-plug has four ports: two fluid ports and two pressure ports. The face of the end-plugs was specifically designed to allow t he injection of two phases into a fracture. Figure 28C presents a photograph of the face of one of the end-plugs. The semi-circular channels at both sides are the entry ports for the two fluids. From these two channels, 0.25 mm channels traverse the face of the end-plug creating an alternating pattern for distributing the fluids into the fracture. Test scans of the new core holder in the high-resolution OMNI-X scanner were acquired. A photograph of the core holder in the scanner is shown in Figure 28, and a sample image of a fracture sample is shown in Figure 30. The high-resolution image allows us to measure fracture aperture with reasonable accuracy while fluids are flowing through the sample.

A

B

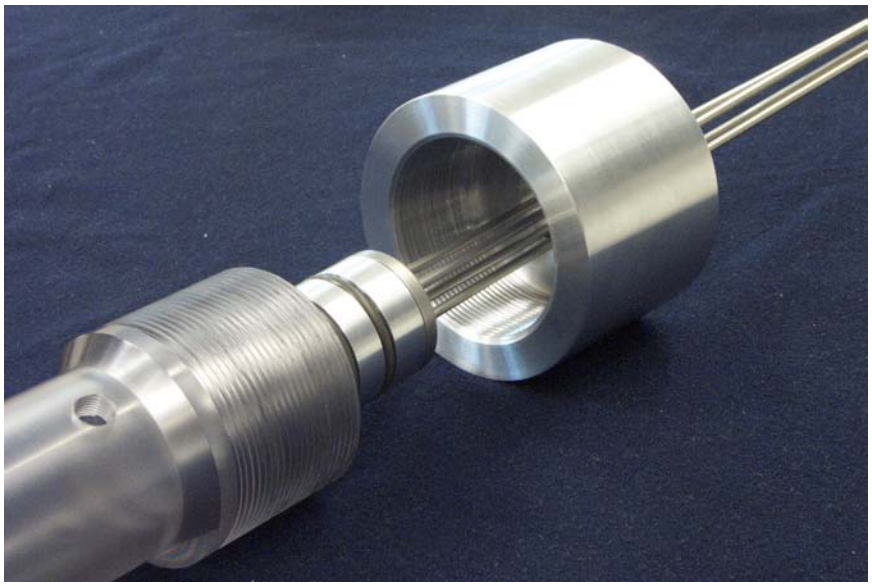

C

Figure 28: Photographs of the new core holder. A: general layout. B: End-plug setup. C: Channels on the injection face of an end-plug.

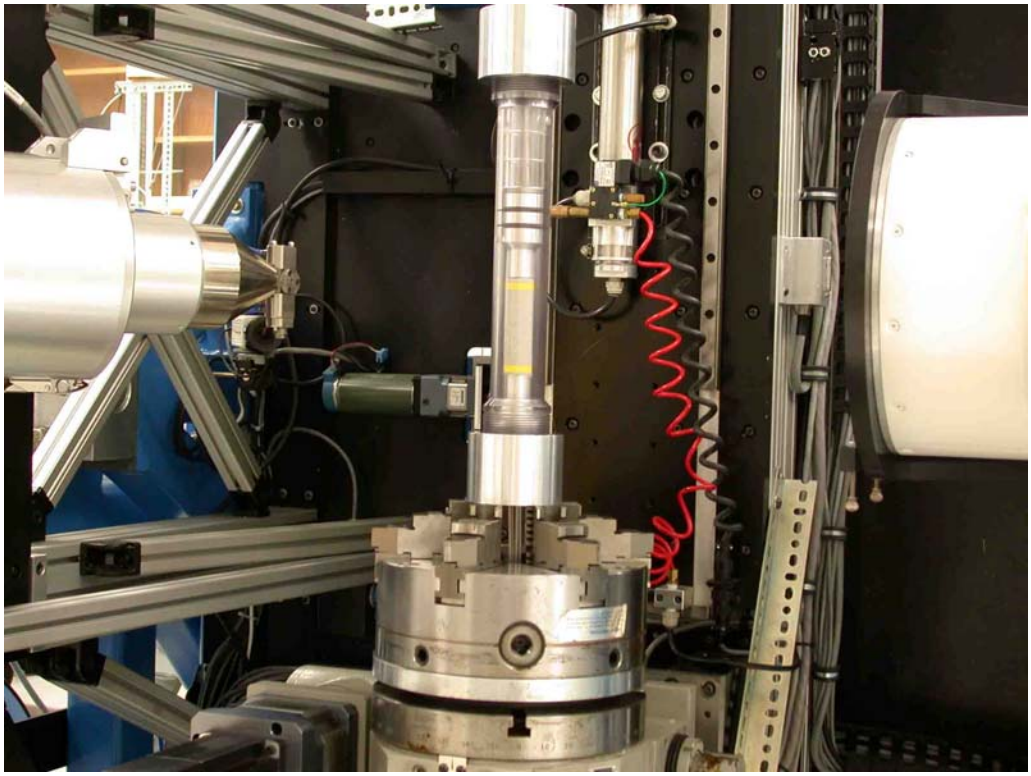

Figure 29: Photographs of the new core holder in the high-resolution OMNI-X scanner.

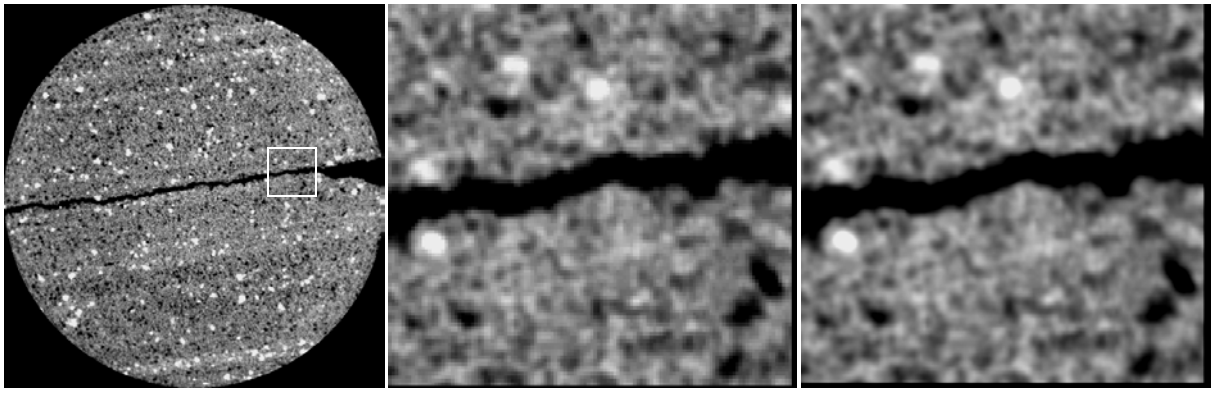

Figure 30: A sample high-resolution image of a fractured sample acquired in the new core holder. A: Entire image (25 mm diameter). B: Pixilated detailed image. C: Smoothed detailed image.

Modeling of Fracture Closure:

Work is continuing on modeling the closure of a fracture in response to confining stress on asperities. A model that combines the solution of silica at the contact points of the asperities and the removal of the dissolved matrix through a thin water film between the grains to the pore space, and the deposition of the solid back on the grains adjacent to the pores is being completed. We expect to show some results in the next report.

Modeling of Fracture-Matrix Fluid Flow Interactions:

The presence of fractures has a significant impact on fluid flow in a porous medium. Two-phase flow experiments are being analyzed in order to understand the flow patterns that develop in the presence of a single fracture in a layered core. The inverse process includes using a numerical fluid flow simulator (Eclipse) to match experimental observations made with x-ray CT. The focus of the work is on extracting relative permeabilities of each layer in a two-dimensional model and then using them in a full three-dimensional model of the entire sample. The three-dimensional simulations are indicating that there is cross flow between the layers in the sample. The fractured Berea sample was divided into fifteen vertical layers perpendicular to the fracture. Layers 8, 9, and 10 were selected to demonstrate the transition from two-dimensional to three-dimensional modeling. Figure 31 shows the average oil saturation after injecting 0.143 pore volumes of oil during the oil loading stage. Each layer was considered as a two dimensional

system. An iterative process was used to optimize the resulting relative permeabilities. Figure 32 shows the average oil saturation along the sample calculated in one three-dimensional simulation. The tow-dimensional parameters were used as the starting point of the three-dimensional simulation. The differences between Figure 31 and Figure 32 indicate that there is cross flow between the layers. The oil loading, or water recovery, from the low permeability layer (9) is slower than the high permeability layers (8, and 10). Figure 33 shows the distribution of oil in layers 8 and 9. The displacement in these layers is influenced by the fracture tip that is close to the center of the sample.

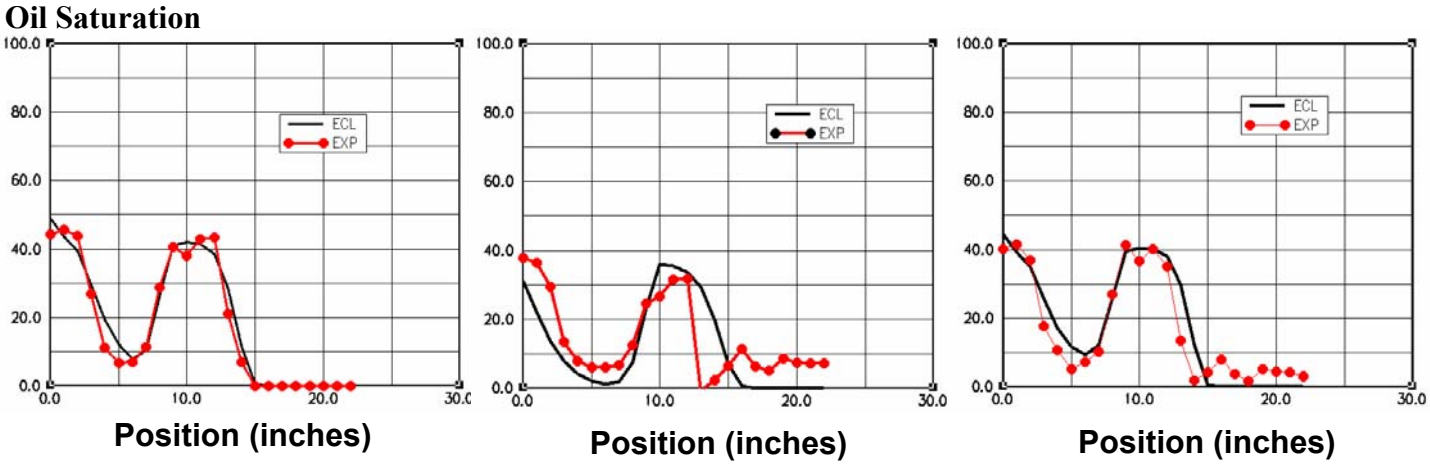

Figure 31: Average oil saturation profiles along the fractured sample resulting from two-dimensional simulation. Left: Layer 8 (high permeability). Middle: Layer 9 (low permeability). Right: Layer 10 (high permeability).

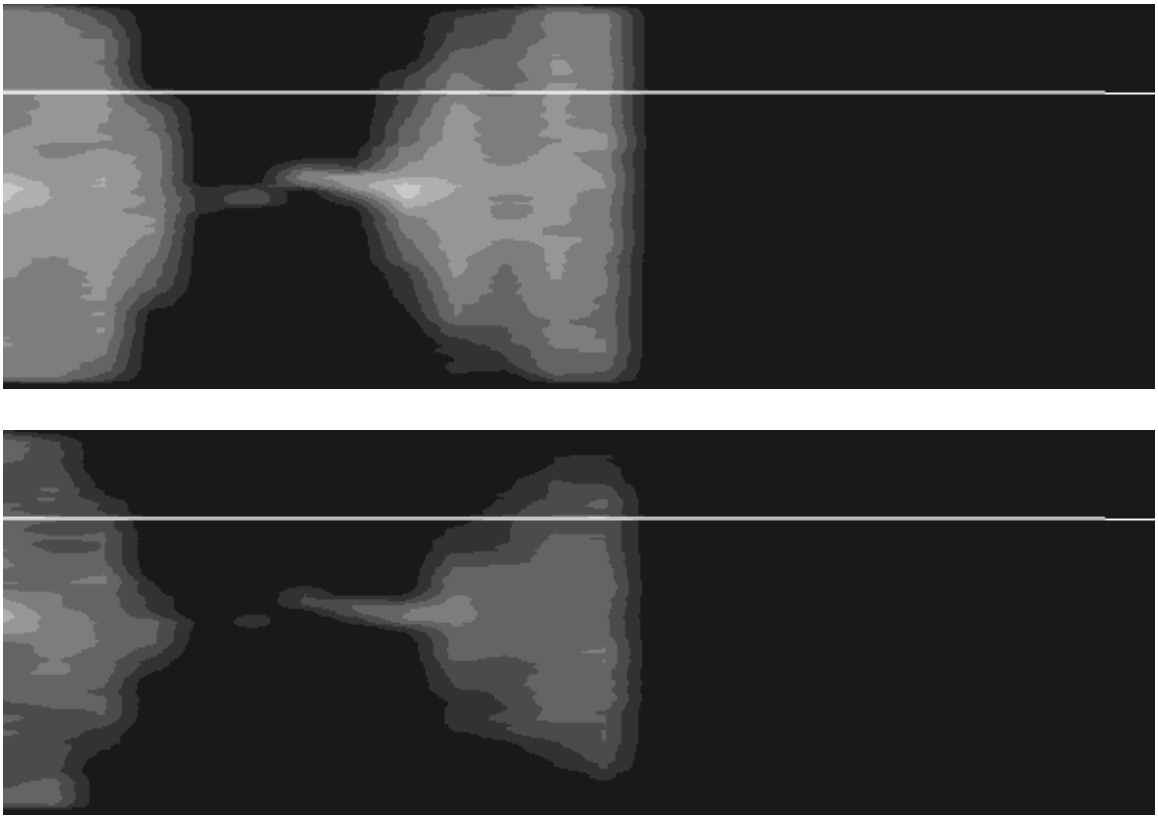

Figure 33: To axial CT sections through the high permeability layer (8) at the top, and the low permeability layer (9) at the bottom.

REFERENCES

Barton, N., S. Bandis and K. Bakhtar, Strength, deformation and conductivity coupling of rock joints. *Int. J. R. Mech*., 22, 121 - 140, 1985

.

Gentier, S., and Hopkins, D., (1997) Mapping fracture aperture as a function of normal stress using a combination of casting, image analysis and modeling techniques, Int. J. Rock Mech. & Min. Sci. 34:3-4, Paper No. 132.

Vinegar, H. J., and Wellington, S. L., Tomographic Imaging of Three-Phase Flow Experiments, Rev. Sci. Insts., January, pp. 96-107, 1987.

LIST OF ACRONYMS AND ABBREVIATIONS